International Journal Of Industrial Electronics Control and Optimization
Print ISSN: 3517-2645
Online ISSN: 3568-2645
Homepage: https://ieco.usb.ac.ir/

Torque Ripple Reduction in Modular Drive of a Non-Sinusoidal, Asymmetric Six-Phase, Permanent Magnet Synchronous Motor with Double Stator Windings using Harmonic Current Injection Strategy

Davood Maleki | Abolfazl Halvaei Niasar

Department of Electrical & Computer Engineering, University of Kashan, Kashan, Iran
Corresponding author's email: halvaei@kashanu.ac.ir

Article Info

Article type:
Research Article

Article history:
Received: 02-April-2025
Received in revised form: 15-May-2025
Accepted: 26-May-2025
Published online: 22-Dec-2025

Keywords:
H-bridge inverter,
Quasi-proportional resonant controller,
Reliability,
Six-phase PMSM.

ABSTRACT

Multiphase permanent magnet synchronous motors (PMSMs) are widely adopted in high-power-density and high-efficiency applications, particularly where reliability is a critical design requirement. This paper presents a control strategy for an asymmetric six-phase PMSM with a dual-winding per-phase stator configuration, where each phase consists of two physically aligned and symmetrically distributed windings relative to the stator center to ensure enhanced drive reliability. The system employs a fully modular control and power architecture, with each winding pair in a phase supplied by an independent single-phase H-bridge inverter. To mitigate torque ripple caused by non-sinusoidal back-EMF waveforms, an optimized harmonic current injection technique is implemented alongside quasi-proportional resonant (QPR) current controllers for precise harmonic compensation. Additionally, under fault conditions (e.g., winding failure), a fault-tolerant control (FTC) algorithm is applied, focusing on the suppression of second-order harmonic torque oscillations to maintain stable operation. The proposed control methodologies are validated through detailed Simulink simulations and further supported by experimental results, confirming their effectiveness in improving performance and reliability.

NOMENCLATURE

e_{x_i}	Back-EMF voltage of winding x_i	v_{x_i}	Voltage of winding x_i
i_{x_i}	Current of winding x_i	i_{y_j}	Current of winding y_j
ψ_{x_i}	Linkage flux of winding x_i	P_{x_i}	Air gap power of the winding x_i
L_{x_i}	Self-inductance of winding x_i	$M_{x_i y_j}$	Mutual inductance between windings x_i and y_j
h	Order of harmonic in currents or back-EMFs	θ_r	Rotor position in electrical rad.
K_P	Proportional gain of PI controller	K_I	Integral gain of PI controller
K_P	Proportional gain of h^{th} harmonic in QPR	K_{Rh}	Resonant gain of h^{th} harmonic in QPR
ω_{ch}	Cut-off frequency of h^{th} harmonic in QPR	ω_o	Resonant frequency in QPR
ω_r	Rotor speed in electrical rad/sec	ω_m	Rotor speed in mechanical rad/sec
T_e	Electromagnetic or airgap torque	P_e	Airgap power
T_e^*	Reference torque	J	Inertia moment
T_l	Electromagnetic load	I_1, I_3, I_5	Injected harmonic current contents
E_1, E_3, E_5	Back-EMF harmonic contents	I_1^*, I_3^*, I_5^*	Reference injected harmonic current contents
T_0, P_0	Constant value of torque/airgap power	T_6, P_6	6^{th} harmonic of torque/airgap power

Publisher: University of Sistan and Baluchestan

I. Introduction

Multiphase electric motors, defined as motors with more than three phases, have gained significant attention from researchers and industry professionals in recent years [1,2]. These motors are commonly used in medium- to high-power applications—such as large ships, submarine, and industrial mills—where enhanced reliability and reduced phase current stress are critical [3,4]. However, realizing these advantages depends on several factors, including motor structure and design. The most common multiphase configurations include 5, 6, 9, and 12-phase systems, with six-phase motors being the most prevalent. Compared to other multiphase motors, six-phase motors offer distinct benefits, such as control simplicity (similar to three-phase systems), ease of design and construction, and straightforward control implementation. As a result, they are widely used in sensitive applications requiring high redundancy, reliability, and fault tolerance, particularly in underwater propulsion systems [5,6].

In critical applications like electric drives for submarines and underwater vehicles, drive reliability is paramount. To ensure robust operation, redundancy is incorporated at both hardware and software levels. Hardware redundancy may involve increasing the number of phases, adding extra power switches, employing independent inverters for each phase, and incorporating redundant sensors and microcontrollers. Additionally, fault-tolerant control (FTC) methods are essential to maintaining uninterrupted operation in the event of a fault [7].

Fig. 1 illustrates the common topology of stator windings in six-phase PMSMs [8], which are classified into two categories: symmetric and asymmetric. In the asymmetric type (Fig. 1(a)), the distance between the axes of two adjacent windings is 30°, whereas in the symmetric type (Fig. 1(b)), it is 60°. Additionally, as seen in Fig. 1(a,b), a six-phase motor can be constructed using two three-phase windings with star connections, leading to its designation as a double-star three-phase PMSM (DTP-PMSM). The star points of these windings may either remain separate or coincide, and in such configurations, two three-phase inverters are typically employed to power the motor.

To enhance reliability, an open-ended connection can replace the double-stranded connection for each winding, as depicted in Fig. 1(c,d). In this setup, each phase is powered by a single-phase H-bridge inverter. For greater reliability, independent local control systems (microcontrollers) can be assigned to each single-phase inverter in the structures shown in Fig. 1(c,d), with an upstream central microcontroller coordinating the operation of all six local microcontrollers. This modular drive topology, featuring separate control and power circuits for each phase, offers a high degree of fault tolerance.

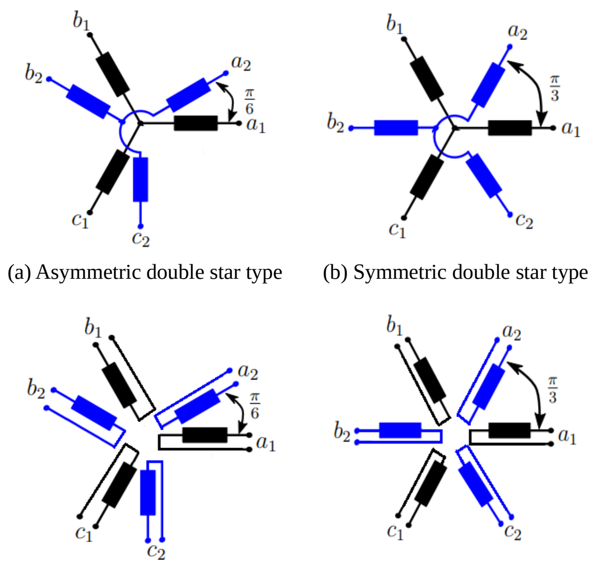

(a) Asymmetric double star type (b) Symmetric double star type

(c) Asymmetric open-end type (d) Symmetric open-end type

Fig. 1. Common types of six-phase PMSMs

In this study, a specialized asymmetric six-phase PMSM is investigated to reduce current stress on the windings and enable higher power output. This motor features a unique stator configuration where each phase consists of two separate windings positioned in two distinct physical halves of the stator, symmetrically arranged around the stator's center. This design can also be termed a six-phase asymmetric motor with dual stator windings. Fig. 2 presents the schematic of the stator winding for this asymmetric six-phase motor with double windings. The windings are connected in an open-end configuration, with each winding in a phase independently controlled by a single-phase H-bridge inverter, all managed by a single microcontroller. Fig. 3 depicts the drive schematic for this modular asymmetric six-phase PMSM with dual stator windings. Notably, the reference currents for both windings of a given phase, sent by the central microcontroller to the corresponding local microcontroller, are identical, ensuring that the resulting MMFs from the two windings remain aligned.

One of the limitations of this structure is that the modular design of the control system prevents data exchange between the local microcontrollers of different phases. As a result, the controllers in each module operate independently without awareness of the voltage and current information from other modules. This restriction poses challenges for modeling and control strategies based on dq reference frame theory, which are commonly applied to three-phase or six-phase motors but rely on certain assumptions about system coupling and information sharing. In the modular drive system under investigation in this research—whose structure is illustrated in Fig. 3—

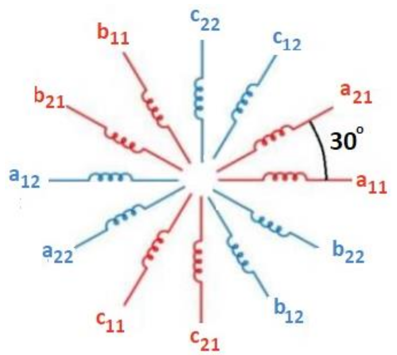

Fig. 2. The schematic of an asymmetric six-phase PMSM with double stator winding

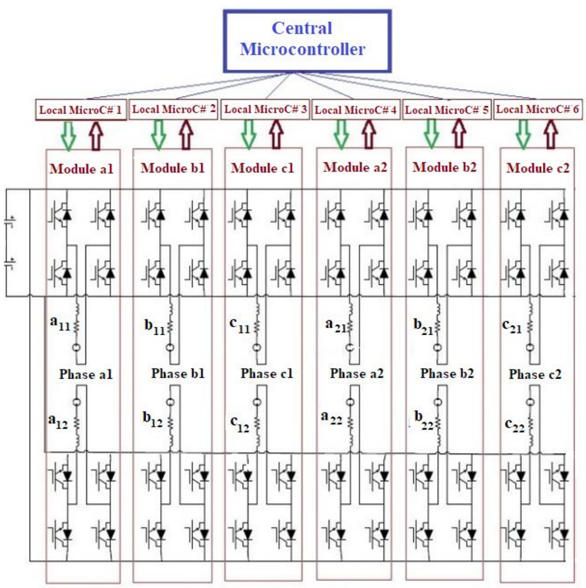

Fig. 3. Schematic of the drive for six-phase, double winding PMSM used in this research

transformations such as 3-to-2 or their inverses cannot be implemented. Consequently, for modeling the modular six-phase PMSM in this study, a six-axis stationary reference frame approach is adopted.

The control methods for three-phase PMSMs are highly diverse. While these methods can also be applied to six-phase PMSMs, their practical use is less common due to the increased number of phases, higher computational burden, processing limitations in microcontrollers, and the poor performance of some methods in high-power motors [9]. Vector control is the most widely used primary method for both three-phase and six-phase PMSMs, offering relatively fast dynamics and smoother torque compared to other approaches. For six-phase PMSMs, vector control is implemented in independent dq frames, decoupled dq frames, and the Vector Space Decomposition (VSD) method. A comparison of various vector control strategies for asymmetric six-phase PMSMs with double-star winding configurations (DTP-PMSM) has been presented in [10]. However, vector control for six-phase PMSMs has several drawbacks, including the computational complexity of Park transformations, challenges in tuning multiple PI controller coefficients, and sensitivity to changes in motor parameters. To address some limitations of vector control, such as the need for multiple PI controllers and their tuning, Direct Torque Control (DTC) has been proposed [11,12]. Nevertheless, DTC also suffers from inherent disadvantages, such as persistent current and torque ripple, along with significant high-frequency noise. Model Predictive Control (MPC) has emerged as an effective and optimal strategy for controlling switching and nonlinear systems, gaining widespread adoption in electric drive applications, including PMSM drives. Several studies have explored MPC for six-phase PMSMs using two-level and three-level inverters [13,14]. However, MPC is also sensitive to parameter variations, and while model-free and robust predictive methods have been proposed for three-phase PMSMs, they have not yet been extended to six-phase PMSMs.

Most conventional control methods rely on motor models in two-axis reference frames, necessitating transformations such as abc-to-dq or αβ. However, in the modular drive structure investigated in this research—where each phase is controlled independently—these conventional methods cannot be applied. In summary, due to the modular architecture of the control system studied here, none of the existing modeling and control methods based on two-axis theory (for either three-phase or six-phase PMSMs) are suitable. Instead, phase-independent modeling and control approaches must be developed.

The primary reason for using multiphase PMSM motors, particularly six-phase motors, is to enhance the fault-tolerant capability and reliability of the drive system under faulty conditions [15]. Fault-tolerant control strategies for six-phase motor drives are crucial to ensure reliable operation under various fault conditions such as open-phase or short-circuit faults. One effective approach is phase redundancy, where healthy phases compensate for faulty ones by redistributing currents, though this may lead to increased torque ripple in severe faults [16]. Model predictive control (MPC) offers dynamic fault handling by optimizing future system behavior, providing excellent performance at the cost of higher computational complexity [17]. Sliding mode control (SMC) is another robust method that maintains stability despite faults by forcing the system into a predefined sliding surface, but its inherent chattering can affect smooth operation [18]. Field-oriented control (FOC) with adaptive current regulation adjusts d-q axis currents to minimize torque disturbances, offering a good balance between performance and simplicity, though it relies heavily on accurate fault detection. Compared to these, MPC and SMC demonstrate superior fault tolerance and adaptability, with MPC being more computationally demanding while SMC suffers from chattering issues [19]. In contrast, FOC and phase redundancy methods are simpler to implement but may lack the same level of precision under extreme fault conditions. The choice of method ultimately depends on the specific application requirements, including computational resources, desired response time, and acceptable torque ripple levels, with advanced methods like MPC being preferred for high-performance applications where reliability is critical [20]. Due to the independent control structure of each phase relative to the others, most aforementioned fault-tolerant control methods relying on dq transformations are not applicable. Therefore, this paper proposes a compensation-based fault-tolerant control strategy for open-circuit faults in one or more windings, which operates independently without requiring dq transformations.

The rest of this paper is organized as follows: Section 2 presents the modeling of the modular non-sinusoidal six-phase PMSM. Section 3 discusses the motor's control using an optimal harmonic current injection strategy with quasi-proportional resonant (QPR) current controllers, followed by a fault-tolerant control method. Simulation results are provided in Section 4, while experimental validation is presented in Section 5. Finally, Section 6 concludes the paper with key findings and insights.

II. Modeling of the Non-Sinusoidal, Asymmetric Six-Phase PMSM with Double Winding

For dynamic modeling of sinusoidal three-phase PMSMs, Park (dq) or Clarke (αβ) transformations are typically employed to represent the system in either rotating or stationary reference frames. Similarly, for six-phase PMSMs, various modeling approaches exist, analogous to those used for three-phase motors. These methods include:

(1) Modeling in independent $\boldsymbol{dq}$ reference frames [21]
(2) Modeling in independent, decoupled $\boldsymbol{dq}$ frames [22]
(3) Modeling using vector space decomposition (VSD) [23]
(4) Modeling in six-axis stationary reference frame [24]

For a six-phase PMSM with sinusoidal back EMF, the first three modeling methods are commonly employed, with no significant difference in computational complexity among them. However, modeling non-sinusoidal PMSMs requires additional considerations when applying these methods. Proposed approaches for modeling non-sinusoidal PMSMs include:

(a) Non-sinusoidal vectorial or extended Park method [25]
(b) Modeling in one dq reference frame considering harmonic components [26]
(c) Modeling in multiple harmonic dq reference frames (MRF) [27]
(d) Vector space decomposition (VSD) method [28]

In the extended Park transformation-based modeling method, the argument and amplitude used in the Park transformation vary according to the rotor angle. When modeling in a single dq reference frame while accounting for harmonic components, the conventional Park transformation is applied, incorporating the effects of harmonic back-EMF voltages in the voltage-current equations and the electromagnetic torque relationship. Alternatively, the multiple harmonic dq reference frames method involves creating rotating dq frames corresponding to the harmonic orders present in the back-EMF voltage, each synchronized to the respective harmonic frequency. The VSD method is one of the most powerful modeling methods that, although originally proposed for modeling sinusoidal multiphase motors, also performs well for modeling non-sinusoidal three-phase motors. In this method, using appropriate 3-to-2 transformations, the main component of the motor signals along with the harmonics of orders $k = 12m \pm 1$ $(m = 1,2,3,\ldots)$ are transferred to the main subspace $\alpha\beta$, while the harmonics of orders $k = 6m \pm 1$ are transferred to the secondary subspace $z1z2$, and the zero-order harmonics $k = 3m$ are mapped to the zero-sequence subspace $o1o2$. The VSD modeling method offers several advantages, including the ability to work with simplified models across three two-dimensional subspaces, facilitating easier controller design and more straightforward harmonic control. Additionally, this method enables the modeling of non-sinusoidal motors—such as those with non-sinusoidal back-EMF voltages—as sinusoidal motors, simplifying analysis and control.

However, both the VSD method and other dq-based modeling techniques are only applicable when the motor employs a centralized control system. Due to the modular structure of the drive system studied in this research, conventional two-axis-based modeling methods cannot be applied. Furthermore, the non-sinusoidal nature of the back-EMF voltages adds to the complexity. Therefore, for the six-phase PMSM with double winding, as illustrated in Fig. 2, modeling in the six-axis stationary reference frame is required. In this approach, the six stationary reference axes are aligned with the winding axes depicted in Fig. 1(c). Assuming the phase naming and arrangement of the PMSM shown in Fig. 2, the voltage-current relationship for each phase is given by:

$$v_{x_i} = R_s i_{x_i} + \frac{d}{dt}\psi_{x_i} + e_{x_i} \tag{1}$$

where R_s is resistance of each stator phase, and v_{x_i} is voltage in the winding x_i, $(x = a, b, c$ & $i = 11,12,21,22)$ and other nomenclature are defined at the beginning of the paper. The value of the flux linkage for each winding depends on the current of that winding and the currents of the other 11 windings, and can be calculated from the following relationship:

$$\psi_{x_i} = L_{x_i} i_{x_i} + \sum_{\substack{y=a,b,c \\ i,j=11,12,21,22 \\ (x_i \neq y_j)}} M_{x_i y_j} i_{y_j} \tag{2}$$

The stator inductance matrix, in the case of the two windings of each phase being separate (for instance, a_{11} and a_{12}) is a 12×12 matrix. Two windings of a phase for improvement the motor performance at low speeds is connected in series and so, the inductance matrix is converted to a 6×6 matrix. The electromagnetic torque T_e and motor speed ω_m for the asymmetric six-phase PMSM with double stator windings can be calculated using as follows:

$$T_e = \sum_{\substack{x=a,b,c \\ i=11,12,21,22}} \frac{e_{x_i} i_{x_i}}{\omega_r} \tag{3}$$

$$\omega_m = \frac{1}{J} \int (T_e - T_l) dt \tag{4}$$

To implement of the model in Simulink, a 12-phase winding can be used, that to each phase, a dependent voltage source with desired harmonic waveform function of rotor position θ_r and amplitude as function of rotor speed, can be added in series.

In the presented motor model in the stationary reference frame with constant inductance values, it is assumed that the rotor is of the surface-mounted permanent magnet type. Additionally, saturation effects and armature reaction are neglected. The presence of these uncertainties and the nonlinear effects manifest themselves in the distortion of the back-EMF voltage waveforms and changes in their harmonic content within the model, which must be taken into account when applying the control method.

III. Control of the Non-Sinusoidal, Asymmetric Six-Phase PMSM with Double Winding using Optimal Harmonic Current Injection Method

In the introduction section it has been explained that due to the modular structure of the drive system under study in this research, the use of control methods based on the two-axis theory is not possible. Moreover, the many numbers of windings and the non-sinusoidal back-EMF voltages also add to the challenge. In this section, to reduce the torque ripple caused by the non-sinusoidal back-EMFs of the windings, an optimal current shaping (or harmonic current injection) strategy is employed in the six-axis stationary reference frame, which will be briefly discussed as follows.

A. Torque Ripple Reduction Using Optimal Harmonic Current Injection Strategy

In harmonic current injection strategy, corresponding to the harmonics present in the phase back-EMF voltages, the fundamental phase current is injected as well as harmonic currents so that the harmonics of torque become zero, leaving only the constant part of the torque [29]. For the six-phase motor in this research, it is assumed that harmonics with orders 1, 3, and 5 are present in the back-EMF voltage. Therefore, the back-EMF voltage of the winding x_i (here $x_i = a_{11}$) can be written as follows:

$$e_{x_i}(t) = E_1 \sin \omega_r t + E_3 \sin 3 \omega_r + E_5 \sin 5 \omega_r t \tag{5}$$

where E_1, E_3, and E_5 are respectively 1, 0.07, and -0.03 per unit in this research. The injected current into winding x_i (here $x_i = a_{11}$) is considered as follows:

$$i_{x_i}(t) = I_1 \sin \omega_r t + I_3 \sin 3 \omega_r t + I_5 \sin 5 \omega_r t \tag{6}$$

For other windings, the argument of the sinusoidal functions changes according to Fig. 1(c). The air gap power of the winding $\boldsymbol{x_i = a_{11}}$ will only include even order harmonics up to the 10th order as follows:

$$P_{x_i}(t) = P_0 + P_2 \sin 2 \omega_r t + \cdots + P_{10} \sin 10 \omega_r t \tag{7}$$

The total air gap power of all windings in a PMSM with phase number multiple of 3, contains only harmonic with orders 6, 12, and 18. Assuming current and voltage harmonics are limited to the 5th order for the motor in this study, the total instantaneous air gap power P_e is obtained as follows:

$$P_e(t) = P_0 + P_6 \sin 6 \omega_r t \tag{8}$$

The instantaneous electromagnetic torque can also be calculated as:

$$T_e(t) = \frac{P_e(t)}{\omega_r} = T_0 + T_6 \sin 6 \omega_r t \tag{9}$$

where:

$$T_0 = \frac{3}{2\omega_r} [E_1 I_1 + E_3 I_3 + E_5 I_5] \tag{10}$$

$$T_6 = \frac{3}{2\omega_r} [-I_1 E_5 + I_3 E_3 - I_5 E_1] \tag{11}$$

To determine the amplitudes of the current harmonics for each phase, by setting $\boldsymbol{T_0}$ equal to the reference torque $\boldsymbol{T_e^*}$ (the output of the speed controller) and setting $\boldsymbol{T_6}$ to zero, the following matrix equation must be solved:

$$\begin{bmatrix} E_1 & E_3 & E_5 \\ -E_5 & E_3 & -E_1 \end{bmatrix} \times \begin{bmatrix} I_1 \\ I_3 \\ I_5 \end{bmatrix} = \frac{2\omega_r}{3} \begin{bmatrix} T_e^* \\ 0 \end{bmatrix} \tag{12}$$

It should be noted that in non-sinusoidal PMSM with the star connection, the third harmonic current cannot flow, and despite the presence of the third harmonic back-EMF voltage, the third harmonic current is not included in the reference current. However, in a motor with an open-end winding, the third harmonic current can flow. One solution—based on the fact that the third harmonic current does not involve in torque generation—is to set the third harmonic current component in the reference current to zero. In this case, in (12), the number of equations and currents becomes equal, allowing the amplitudes of the current harmonics to be determined. However, if the third harmonic is considered, it can be adjusted in such a way that the total RMS current (and thus copper losses) is minimized. In this case and in (12), the number of unknown currents is 3 that is more than the number of equations. This refer that it has not a unique solution. Hence, an optimization must be performed to extract the best solution. An optimal method to solve this equation is such that, in addition to satisfying the above equations, the rms value of the current vector $\boldsymbol{I} * \boldsymbol{I^t}$ should be also minimized, thereby obtaining the optimal harmonic values of the current. Thus, consider the following optimization problem [30]:

$$\begin{aligned} &Minimize\ \ C = xx^T \\ &x = [I_1 \quad I_3 \quad I_5] \\ &if; Ax = B \\ &B = \frac{2\omega_r}{3}\begin{bmatrix} T_e^* \\ 0 \end{bmatrix},\ A = \begin{bmatrix} E_1 & E_3 & E_5 \\ -E_5 & E_3 & -E_1 \end{bmatrix} \end{aligned} \tag{13}$$

The optimal solution of above problem is obtained as follows [37]:

$$x_{opt} = A^T \times (A \times A^T)^{-1} \times B \tag{14}$$

Using the above solution, the optimal values of the current harmonic amplitudes are obtained as follows:

$$\begin{bmatrix} I_1^* \\ I_3^* \\ I_5^* \end{bmatrix} = \begin{bmatrix} 0.9956 \\ 0.0736 \\ 0.0247 \end{bmatrix} \frac{2\omega_r T_e^*}{3} \tag{15}$$

B. Harmonic Current Regulation for Windings using Proportional-Resonant Controllers

Using (6) and (15), the time relation of the reference current for both windings of the phase $\boldsymbol{a_1}$, based on the reference torque, can be determined as follows:

$$i_{a_1}^*(t) = I_1^* \sin\omega_r t + I_3^* \sin 3\,\omega_r t + I_5^* \sin 5\,\omega_r t \tag{16}$$

The current of phase $\boldsymbol{a_1}$ windings, in all transient and steady states, must accurately track the aforementioned reference value. For this purpose, appropriate current controllers should be used. The simplest type of controller is the hysteresis controller, which, due to its steady-state error in current and high, and variable switching frequency, is not suitable for high-power applications sensitive to acoustic noise. On the other hand, the traditional PI controller is also not suitable for this application because the PI controller, due to its small bandwidth, is not capable of tracking AC signals containing high-order harmonics [31]. An effective and suitable solution for tracking harmonic reference signals is the using of proportional-resonant (PR) controllers or quasi-proportional-resonant (QPR) controllers. The transfer function of the QPR controller can be expressed as:

$$G_{QPR}(s) = K_P + K_R \frac{2\omega_c s}{s^2 + 2\omega_c s + \omega_o^2} \tag{17}$$

The QPR controller has four parameters: ω_o, ω_c, K_P, and K_R, which must be correctly chosen. The resonance frequency ω_o is exactly equal to the fundamental system's sinusoidal signal frequency. However, the other three parameters should be selected to maximize the gain around the resonance frequency while appropriately attenuating neighboring frequencies. There are various methods for designing and determining the parameters of QPR controllers, the most important of which are: (i) trial-and-error method, (ii) the forced oscillation method (time domain), (iii) the frequency response method (frequency domain).

The trial-and-error method involves manually adjusting the gains and controller parameters and observing the motor's response to various input signals that is briefly presented [31]. (1) Selecting initial values; Choose initial values for the parameters K_R, K_P, and ω_c based on prior experience or knowledge of the PMSM drive system. These initial values serve as the starting point for the tuning process. (2) Tuning the proportional gain K_P; First, adjust the proportional gain K_P to achieve the desired steady-state performance. This can be done using methods such as trial and error or systematic tuning approaches like the Ziegler-Nichols method. (3) Tuning the resonance gain K_R; After tuning the K_P, adjust the K_R to achieve the desired tracking performance. This can also be done using trial and error or systematic tuning methods such as the Internal Model Control (IMC) method. (4) Tuning the cut-off frequency ω_c; adjust the ω_c to achieve the desired compromise between dynamic response and stability. This can be done by observing the system's step response to a reference current and adjusting ω_c to achieve the desired settling time and overshoot, (5) Validating the tuned parameters; evaluate the controller's performance under various operational conditions and disturbances to ensure it meets the desired performance criteria.

If, in addition to fundamental signal with frequency ω_o, the higher-order harmonics of the signal are available, the QPR controller should be modified. For reference harmonic current given by (16), the transfer function of the QPR controller can be expressed as follows:

$$G_{QPR,H}(s) = K_P + K_{R_1}\frac{2\omega_{c_1}s}{s^2 + 2\omega_{c_1}s + {\omega_o}^2} + K_{R_3}\frac{2\omega_{c_3}s}{s^2 + 2\omega_{c_3}s + (3\omega_o)^2} + K_{R_5}\frac{2\omega_{c_5}s}{s^2 + 2\omega_{c_5}s + (5\omega_o)^2} \quad (17)$$

The optimal values for the parameters K_P, K_{R_h}, and ω_{c_h} for the six-phase motor drive in this research are determined using the trial-and-error method.

Fig. 4 illustrates the block diagram of the six-phase PMSM control system in this paper using harmonic current injection strategy as well as QPR controllers for winding current regulation. A PI controller generates the reference torque based on tracking error of speed. Using harmonic current injection strategy and based on eq. (15) the current reference for all phases is determined and finally by 12 QPR controllers, the current regulation is implemented.

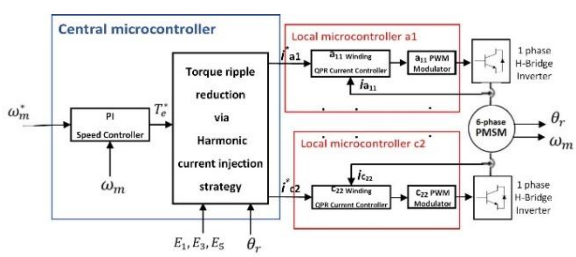

Fig. 4. Schematic of control system for the six-phase PMSM with double windings using harmonic current injection strategy

C. Motor Control Under Single-Phase Fault

The modular six-phase PMSM with open-end winding configuration provides the best control capabilities under fault conditions compared to other 6-phase or even 12-phase motors with star- connections. It has the ability to eliminate torque ripple using the allowable current capacity of the remaining healthy phases for each fault condition. In healthy condition, ignoring the effect of high frequency switching and cogging, the developed electromagnetic torque is constant and free of any oscillations. However, when a fault occurs in one or more windings, the generated torque becomes oscillatory, adding a second harmonic oscillatory torque component to the constant torque. The fault-tolerant control (FTC) strategy used in this study is based on reconstructing the amplitude and angle of the main harmonic current of one or some healthy windings to re-establish the balance between the second harmonic torques of the healthy winding [32]. To demonstrate the proposed FTC, assume that the back-EMF voltage and current of the windings of the six-phase shown in Fig. 1 are sinusoidal. The air-gap powers resulting from six-windings $a_{11}b_{11}c_{11}a_{21}b_{21}c_{21}$ (group 1) can be obtained as follows:

$$\begin{aligned}
P_{a_{11}}(t) &= \frac{E_1 I_1}{2} + \frac{E_1 I_1}{2}cos(2\omega_r t) \\
P_{a_{21}}(t) &= \frac{E_1 I_1}{2} + \frac{E_1 I_1}{2}cos(2\omega_r t + 60^o) \\
P_{b_{11}}(t) &= \frac{E_1 I_1}{2} + \frac{E_1 I_1}{2}cos(2\omega_r t + 120^o) \\
P_{b_{21}}(t) &= \frac{E_1 I_1}{2} + \frac{E_1 I_1}{2}cos(2\omega_r t + 180^o) \\
P_{c_{11}}(t) &= \frac{E_1 I_1}{2} + \frac{E_1 I_1}{2}cos(2\omega_r t + 240^o) \\
P_{c_{21}}(t) &= \frac{E_1 I_1}{2} + \frac{E_1 I_1}{2}cos(2\omega_r t + 300^o)
\end{aligned} \quad (18)$$

From the above relationships, it is observed that the air-gap power and consequently the electromagnetic torque of each windings includes a second harmonic oscillatory component, and the sum of these oscillations in the six windings is zero. Fig. 5(a) shows the direction of the six-phase motor current vector, and Fig. 5(b) shows the corresponding second harmonic torque vectors generated by each phase in the healthy condition. It is observed that the sum of all the second harmonic torque vectors in Fig. 5(b) is zero. This balance is there for the second windings of phases $a_{12}b_{12}c_{12}a_{22}b_{22}c_{22}$ (group 2). When one or more windings fails, the balance between the second harmonic torques is disturbed, and torque ripple occurs.

With an open-circuit fault in the a_{11} winding of phase a_1 or corresponding H-bridge inverter, this winding is not capable of producing torque. Hence, the second harmonic oscillatory component in the total torque is created. In other words, as shown in Fig. 6(a), with the lack of the second harmonic torque vector of the a_{11} winding, the balance of the remaining 5 vectors is disrupted. To re-establish balance between these 5 remaining vectors, the directions of the two remaining windings in this three-phase group (b_{11} and c_{11}), must be aligned. For this purpose, their angles can be changed by -30° and $+30^{\circ}$ respectively, or only the direction of one of them (for example c_{11}) can be changed by $+60^o$. Here, the second solution is chosen, that the new current vector c'_{11} is obtained as shown in Fig. 6(b). It is clear that three vectors $a_{21}b_{21}c_{21}$ are balanced with each other, and two vectors $b_{11}c'_{11}$ are balanced as well. Also, the amplitudes of all windings are adjusted to appropriate and permissible values to meet the load torque requirements.

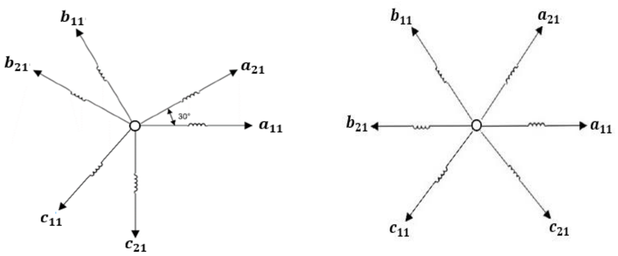

(a) Main harmonic of current (b) Second harmonic of torque

Fig. 5. Current and torque vectors of each phase in the open-ended winding, asymmetrical six-phase PMSM

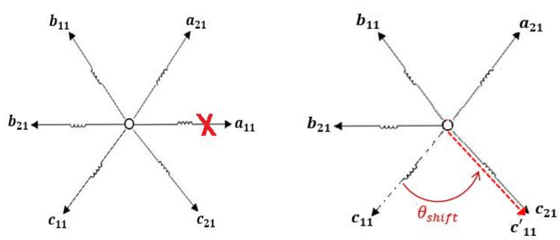

(a) Fault condition (b) Fault compensation

Fig. 6. Single-phase fault compensation in a modular six-phase PMSM (in group 1) by shifting angle current of c_{11} by +60°

There are six possible single-phase faults for each six-phase group, which are described in Table I along with their compensation methods. The proposed FTC method does not consider the source of the fault, which could be a short circuit in the single-phase H-bridge inverter of any winding, an open-circuit fault in the winding, a short-circuit fault in the winding, or even a fault in the microcontroller of any phase. It is based on measuring the effective current of each winding, which becomes zero.

TABLE I. VARIOUS SCENARIOS OF SINGLE-PHASE FAULT IN GROUP 1 AND COMPENSATOR (CORRECTED) WINDING

Faulty winding	Corrected winding	Angle shift
a_{11}	c_{11}	$+60^o$
b_{11}	a_{11}	$+60^o$
c_{11}	b_{11}	$+60^o$
a_{21}	b_{21}	$+60^o$
b_{21}	c_{21}	$+60^o$
c_{21}	a_{21}	$+60^o$

D. Motor Control Under Multiple-Phases Fault

In the case of faults in multiple windings, such as faults in two or more windings, a similar FTC method can be applied without any specific limitations. Generally, for n-phase fault scenario, the number of fault conditions in each group of 6 windings equals the combination $\binom{6}{\mathrm{n}}$. Therefore, the number of possible fault conditions for 2, 3, 4, and 5 windings is 6, 15, 20, 15, and 6, respectively. The total number of possible fault conditions employed motor in this research in each group is 62, and for both groups, it is 124. For each condition, the compensating phases can be easily determined. Table II lists the 15 different fault scenarios occurring in two windings, including the compensating winding. The same FTC method, based on balancing the second torque harmonics in healthy phases, remains applicable. Please note that in some fault conditions, such as faults in two windings a_{11}, c_{21}, the balance of the second-harmonic torque vectors in the remaining healthy windings is inherently maintained and does not require compensation.

IV. Simulation Results

In this section, for the double-winding six-phase PMSM with rated specifications 200 kW, 245 V, $R_s = 50\,m\Omega$, $L_s = 232\,0\mu H$, back-EMF voltage constant $1.37\,rad/s$, and inertia $0.1\,kg \cdot m^2$, the motor behavior is compared using the harmonic current injection control method and two types of current controllers, quasi-proportional-resonant (QPR) and PI, through simulation.

TABLE II. VARIOUS SCENARIOS OF TWO-PHASE FAULT IN GROUP 1 AND COMPENSATOR (CORRECTED) WINDINGS

Faulty winding	Corrected winding	Angle shift
a_{11}, b_{11}	b_{21}	$+60^o$
a_{11} c_{11}	c_{21}	$+60^o$
b_{11}, c_{11}	a_{21}	$+60^o$
a_{21}, c_{21}	a_{11}	$+60^o$
a_{21}, b_{21}	c_{11}	$+60^o$
b_{21}, c_{21}	b_{11}	$+60^o$
a_{11}, a_{21}	c_{11}	$+120^o$
a_{11}, b_{21}	c_{21}	$+120^o$
a_{11}, c_{21}	No compensation needed	
b_{11}, a_{21}	b_{21}	$+120^o$
b_{11}, b_{21}	No compensation needed	
b_{11}, c_{21}	a_{11}	$+120^o$
c_{11}, a_{21}	No compensation needed	
c_{11}, b_{21}	b_{11}	$+120^o$
c_{11}, c_{21}	a_{21}	$+120^o$

The gains of the QPR controllers for all phases are set to $K_P = 35$, $K_{R1} = 10$, $K_{R3} = 0.1$, $K_{R5} = 0.1$, and $\omega_{ci} = 10$. Fig. 7 shows the behavior of the drive in tracking the reference speed and under an increasing load torque proportional to the square of the speed $T_l = 6.43\omega_m^2$. The reference speed is 120 rpm, and the load torque at this speed is approximately $1000\,N \cdot m$. The reference speed tracking error is very small and below 0.5%. The fourth chart in Fig. 7 shows the waveform of the non-sinusoidal back-EMF voltages of the motor. The current winding a_{11} accurately follows the non-sinusoidal reference current using QPR current controllers, with minimal torque ripple of about 3%, as shown in the third chart in Fig. 7.

Fig. 8 shows the drive behavior using PI current controllers, where the gain values of the controllers for all phases are set to $K_I = 100$ and $K_P = 20$. It is observed that this type of controller, due to bandwidth limitations, cannot accurately track the harmonic reference current. Hence, the PI controller is not suitable. Also, the hysteresis current controller, due to the excessively high and variable unacceptable switching frequency, exhibits similar behavior to the PI controller. Therefore, the QPR controller, is a suitable type of controller for phase current regulation in the modular six-phase motor drive system that using harmonic current injection.

To investigate the performance of the proposed fault-tolerant control (FTC), the drive behavior under single-phase fault windings a_{11}, is examined through simulation.

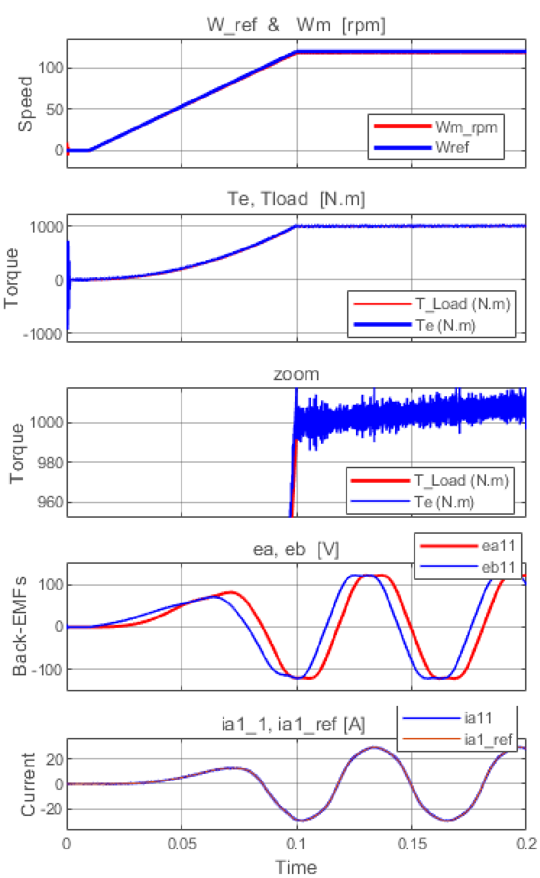

Fig. 7. Drive behavior using QPR current controllers at nominal speed and under nominal load torque.

According to Fig. 9, it is assumed that winding a_{11} experiences a fault at 0.2 seconds. According to the fourth chart in Fig. 9, the developed torque experiences oscillations with the second harmonic order of the stator current. These oscillations, as shown in the second chart, results in oscillations in the motor speed. According to the current charts in Fig. 9, the amplitude of the healthy winding currents (e.g. a_{11}) increases slightly after the fault occurrence to develop the load demanded torque. At 0.3 seconds, fault compensation is carried out by adjusting the current angle of the healthy winding c_{11} by 60º as shown in Fig. 6(b). It is observed that the amplitude of the windings' current increases after compensation at 0.3 sec due to phase difference between the current and back-EMF voltage of winding c_{11}. Moreover, the torque and speed oscillations decrease after this compensation. After compensation, the phase difference between currents of c_{11} and c_{12} windings increase to 60º as shown in sixth chart in Fig. 9. Also, as shown in last chart in Fig. 9, phase difference between currents of c_{11} and b_{11} windings decrease from 120º to 60º.

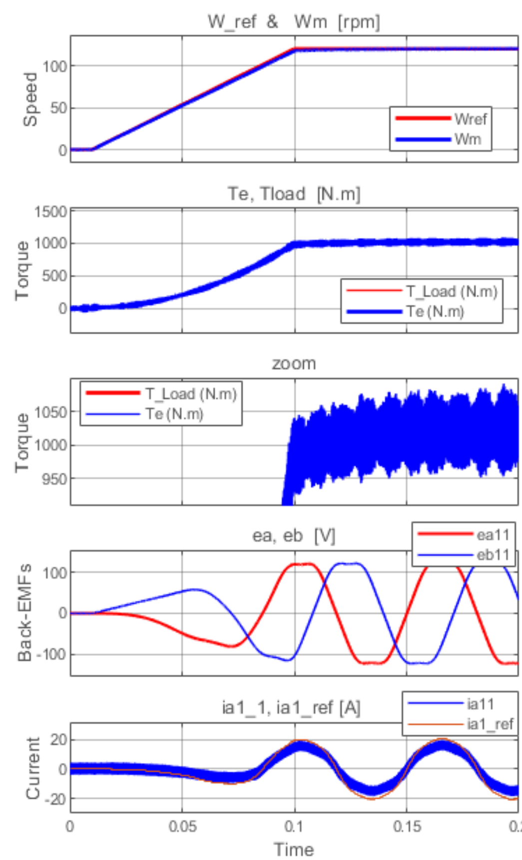

Fig. 8. Drive behavior using PI current controllers at nominal speed and under nominal load torque.

V. Experimental Results

To confirm the proposed control methods in healthy and fault conditions for the double-winding six-phase PMSM drive, some practical tests were conducted on the laboratory setup using the 200 kW double-winding six-phase PMSM. The schematic of the setup is shown in Fig. 10, where seven microcontrollers type STM32F407VGT6 have been used as central and local controllers. The drive of each phase consists of a microcontroller board as well as double H-bridge single-phase inverters and a separate excited DC generator is employed as load. The parameters for all winding QPR controllers are the same and, according to (17), are $K_P = 1$, $K_{R1} = 15$, $K_{R3} = 0.1$, $K_{R5} = 0.1$, and $\omega_{ci} = 10$.

Fig. 11 shows the speed response of the motor using the harmonic current injection strategy as well as QPR controllers for current regulation and a PI controller for speed regulation. The reference speed is 120 rpm and the tracking is satisfactorily performed.

Fig. 12 shows the harmonic current of winding c_{11} as well as expanded speed, that the speed ripple ($\Delta\omega_m$) in this condition is equal to 1 rpm. Fig. 13 illustrates the current waveforms of three windings $a_{11}b_{11}c_{11}$.

Fig. 14 shows the results of the practical test where open circuit fault has occurred in winding a_{11} and the fault tolerant control method has not yet been applied. The speed reference is 40 rpm. It can be seen that due to the torque ripple created, the speed fluctuation becomes very large and reaches a value of 9 rpm, which is about 22.5% of the rated speed.

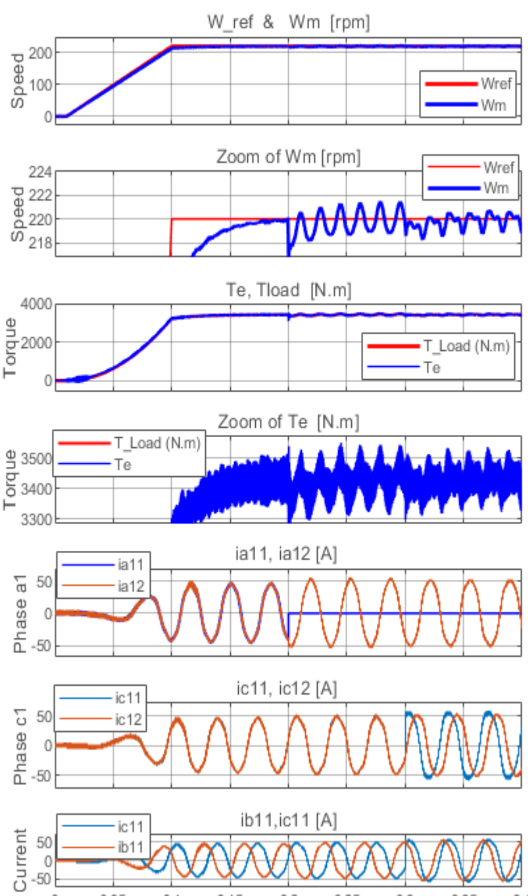

Fig. 9. Drive behavior under single-phase fault of winding a_{11} at 0.2 sec and compensation by adjusting the current angle of winding c_{11} at 0.3 sec by 60°

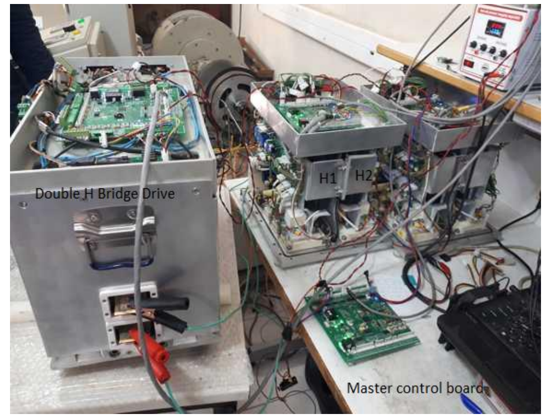

Fig. 10. Experimental setup of modular six-phase PMSM drive

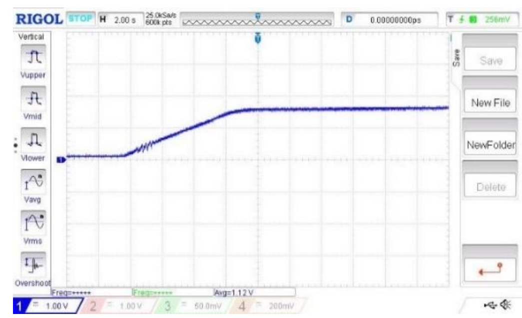

Fig. 11. Motor speed response with using harmonic current injection in healthy condition

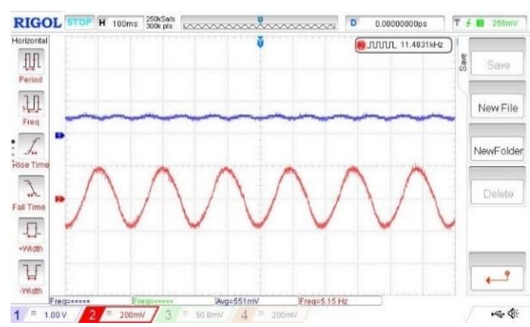

Fig. 12. Current of winding $\boldsymbol{c_{11}}$ (red) as well as enlarged speed waveform (blue) with using harmonic current injection in healthy condition of the motor

Fig. 15 shows the practical results for applying the proposed FTC method under open circuit single-phase fault in winding a_{11}. As mentioned in section 3.C and according to Fig. 6, to re-establish balance between five remaining vectors, the direction of c_{11} must be shifted by +60°, resulting in the new current vector c'_{11}. Fig 15(a) shows the motor speed and current of winding c'_{11}. The speed fluctuation decreases to 5 rpm, which means 10% improvement in speed fluctuations. Fig. 15(b) shows the

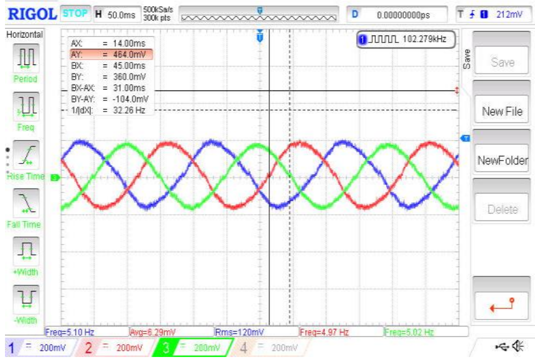

Fig. 13. Currents of three windings $\boldsymbol{a_{11} b_{11}}$ and $\boldsymbol{c_{11}}$ by using harmonic current injection strategy in healthy condition of the motor

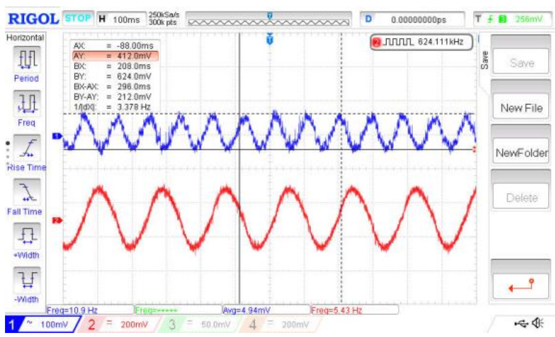

Fig. 14. Motor speed (blue) and current (red) of winding c_{11} during single-phase fault in winding a_{11} **without** compensation

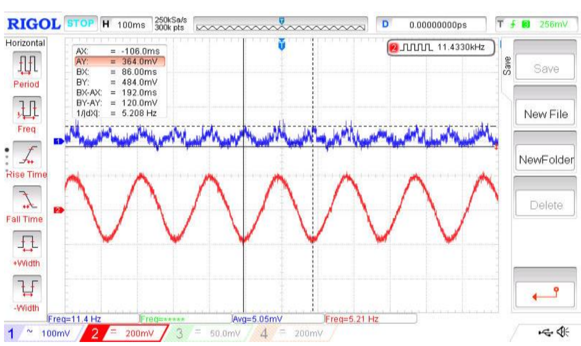

(a) Motor speed (blue) and current (red) of winding c_{11}

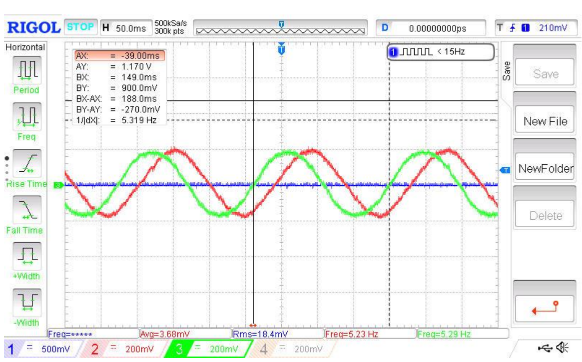

(b) The currents of winding c'_{11} (shifted of c_{11}) and b_{11}

Fig. 15. Behavior of the drive during single-phase fault in winding a_{11} **with** compensation by adjusting the angle of current in c_{11}

currents of two windings c'_{11} and b_{11}, which are observed to have a phase difference of 60° with respect to each other, while in the healthy condition, their difference is 120°.

VI. Conclusions

In this study, torque ripple reduction in a six-phase PMSM with a fully modular drive system was investigated. Due to the modular architecture of the drive's control system, modeling was conducted in a six-axis stationary reference frame, with each phase controlled independently in its stationary reference frame. To address non-sinusoidal back-EMF voltage, an optimized harmonic current injection strategy was proposed, minimizing the effective current amplitude and associated losses while eliminating torque harmonics. Harmonic quasi-proportional-resonant (QPR) current controllers were employed to track the harmonic reference currents, demonstrating highly effective performance. Furthermore, to mitigate torque ripple under single-phase fault conditions, a fault-tolerant control (FTC) strategy was introduced. This method balances the second harmonic of torque generated by the interaction of the fundamental harmonic of current and back-EMF voltage. However, it should be noted that the proposed FTC cannot fully eliminate the second harmonic torque component arising from higher-order current and back-EMF harmonics. It is also worth mentioning that this method has no specific limitation for being extended to higher-power motors. Its only dependency is on the harmonic content of the motor's back-EMF voltages, which may not remain constant at higher power levels. In such cases, the harmonic content must be estimated online. The presented FTC method can also be extended to multi-phase fault scenarios.

References

[1] M. Furmanik, L. Gorel, D. Konvi, P. Rafajdus, "Comparative Study and Overview of Field-Oriented Control Techniques for Six-Phase PMSMs", *Applied. Science*, vol. 11, no. 7841, pp. 1-16, 2021, [**DOI:**10.20944/preprints202108.0022.v1]

[2] K.S. Khan, W.M. Arshad, S. Kanerva, "On performance figures of multiphase machines", *IEEE 18th International Conference on Electrical Machines*, 2008. [**DOI:** 10.1109/ICELMACH.2008.4799836]

[3] J.R. Fu, T.A. Lipo, "Disturbance-free operation of a multiphase current-regulated motor drive with an opened phase", *IEEE Trans. on Ind. Appl.*, vol. 30, pp. 1267–1274, 1994. [**DOI:** 10.1109/28.315238]

[4] S. Kuznetsov, "Machine design and configuration of a 7000 hp hybrid electric drive for naval ship propulsion", *IEEE International Electric Machines & Drives Conference*, 2011. [**DOI:** 10.1109/IEMDC.2011.5994605]

[5] J.F. Hansen, F. Wendt, "History and state of the art in commercial electric ship propulsion, integrated power

systems, and future trends”, *Proceedings of IEEE*, vol. 103, pp. 2229–2242, 2015.
[**DOI:** 10.1109/JPROC.2015.2458990]

[6] J. Rahmanifard, “Design Optimization and Thermal Analysis of a Dual Three-Phase PM Motor for Electric Vehicles, International Journal of Industrial Electronics, Control and Optimization”, Articles in Press, Available Online from 03 May 2025,
[**DOI:** 10.22111/ieco.2025.51426.1674]

[7] J.S. Thongam, M. Tarbouchi, A.F. Okou, D. Bouchard, R. Beguenane, “Trends in naval ship propulsion drive motor technology”, *IEEE Electrical Power & Energy Conference*, 2013.
[**DOI:** 10.1109/EPEC.2013.6802942]

[8] D. Benatti, C. Alosa, E. Carfagna, F. Immovilli, E. Lorenzani, “Assessment of Master-Slave and Droop Control Strategies in Multi-Three-Phase Drives”, *IEEE Workshop on Electrical Machines Design, Control and Diagnosis (WEMDCD)*, pp. 163-168, 2021.
[**DOI:** 10.1109/WEMDCD51469.2021.9425685]

[9] Z. Zhu, S. Wang, B. Shao, L. Yan, P. Xu, Y. Ren, “Advances in Dual-Three-Phase Permanent Magnet Synchronous Machines and Control Techniques,” *Energies*, vol. 14, no. 7508, pp. 1-46, 2021.
[**DOI:**10.3390/en14227508]

[10] M. Furmanik, L. Gorel, D. Konvi, P. Rafajdus, “Comparative Study and Overview of Field-Oriented Control Techniques for Six-Phase PMSMs”, *Applied. Science*, vol. 11, no. 7841, pp. 1-16, 2021.
[**DOI:**10.20944/preprints202108.0022.v1]

[11] Y. Ren, Z.Q. Zhu, “Enhancement of steady-state performance in direct torque controlled dual-three phase permanent magnet synchronous machine drives with modified switching table”, *IEEE Trans. Ind. Electron*. vol. 62, pp. 3338–3350, 2015
[**DOI:** 10.1109/TIE.2014.2376881]

[12] Y. Ren, Z.Q. Zhu, J.E. Green, Y. Li, S. Zhu, Z. Li, “Improved duty-ratio-based direct torque control for dual three-'phase permanent magnet synchronous machine drives”, *IEEE Trans. Ind. Appl*. vol. 55, pp. 5843–5853. 2019.
[**DOI:** 10.1109/TIA.2019.2938468]

[13] T. Luan, Z. Wang, Y. Long, Z. Zhang, Q. Li, “Multi-Virtual-Vector Model Predictive Current Control for Dual Three-Phase PMSM”, *Journals of Energies*, vol. 14, no. 21, 2021.
[**DOI:** 10.3390/en14217292]

[14] S.W. Hwang, D.K. Son, S.H. Park, G.H. Lee, Y.D. Yoon, M.S. Lim, “Design and Analysis of Dual Stator PMSM With Separately Controlled Dual Three-Phase Winding for eVTOL Propulsion”, *IEEE Trans. on Transportation Electrification*, vol. 8, no.4, pp. 4255-4264, 2022.
[**DOI:** 10.1109/TTE.2022.3192353]

[15] E. Levi, “Multiphase Electric Machines for Variable-Speed Applications, IEEE Press, 2018,
[**DOI:**10.1109/TIE.2008.918488]

[16] W. Lee, S.G. Min, B. Sarlioglu, “Fault-Tolerant Operation of Six-Phase Permanent Magnet Motor Drive with Open-Circuit Failures”, IEEE Trans. on Transportation Electrification, vol. 10, no. 3, pp. 5910-5920, 2024,
[**DOI:** 10.1109/TTE.2023.3326089]

[17] F.C. Gonçalves Pedro, M.A. Cruz Sérgio, M.S. Mendes André, “Fault-Tolerant Predictive Current Control of Six-Phase PMSMs With Minimal Reconfiguration Requirements”, IEEE Journal of Emerging and Selected Topics in Power Electronics, vol. 11, no. 2, pp. 2084-2093, 2023,
[**DOI:** 10.1109/JESTPE.2022.3223515]

[18] F.J. Lin, Y.C. Hung, M.T. Tsai, “Fault-Tolerant Control for Six-Phase PMSM Drive System via Intelligent Complementary Sliding-Mode Control Using TSKFNN-AMF”, IEEE Trans. on Industrial Electronics, vol. 60, no. 12, pp. 5747-5762, 2013,
[**DOI:** 10.1109/TIE.2013.2238877]

[19] F. Baneira, J. Doval-Gandoy, A.G. Yepes, O. López, D. Pérez-Estévez, “Comparison of Postfault Strategies for Current Reference Generation for Dual Three-Phase Machines in Terms of Converter Losses”, IEEE Trans. on Power Electronics, vol. 32, no. 11, pp. 8342-8346, 2017,
[**DOI:** 10.1109/TPEL.2017.2691401]

[20] A. Mohammadpour, L. Parsa, “Global Fault-Tolerant Control Technique for Multiphase Permanent-Magnet Machines”, IEEE Trans. on Industry Applications vol. 51, no. 1, pp. 178-186, 2014,
[**DOI:** 10.1109/TIA.2014.2326084]

[21] 8F. Barrero, M.J. Duran, “Recent Advances in the Design, Modeling, and Control of Multiphase Machines—Part I”, *IEEE Trans. on Industrial Electronics*, vol. 63, no. 1, pp. 449-458, 2016.
[**DOI:** 10.1109/TIE.2015.2447733]

[22] S. Kallio, M. Andriollo, A. Tortella, J. Karttunen, “Decoupled d-q Model of Double-Star Interior-Permanent-Magnet Synchronous Machines”, *IEEE Trans. on Industrial Electronics*, vol. 60, no. 6, pp. 2486-2494, 2013.
[**DOI:** 10.1109/TIE.2012.2216241]

[23] Y. Hu, Z.Q. Zhu, M. Odavic, “Comparison of Two-Individual Current Control and Vector Space Decomposition Control for Dual Three-Phase PMSM”, *IEEE Trans. on Industry Application*, vol. 53, no. 5, pp. 4483-4492, 2017.
[**DOI:** 10.1109/TIA.2017.2703682]

[24] A.H. Almarhoon, “Sensorless Control of Dual Three-phase Permanent Magnet Synchronous Machine Drives”, *Ph.D. Thesis, The University of Sheffield*, 2016.
[**DOI :10.3390/en16031326**]

[25] L.R. Rocha, E.C. Silva, P.H.A. Silva, G.X. Prestes, B.C.R. Cordeiro, L.F. Pessoa, R.P. Vieira, “Evaluation Methodology of Current Control Techniques for Torque Ripple Reduction in Non-Sinusoidal PMSM”, *IEEE 8th Southern Power Electronics Conference (SPEC)*, 2023.
[**DOI:**10.1109/SPEC56436.2023.10407773]

[26] M.J. Nam, J.H. Kim, K.Y. Cho, H.W. Kim, Y. Cho, “Torque Ripple Reduction of an Interior PM Synchronous Motor by Compensating Harmonic Currents Based on Flux Linkage Harmonics*”, Journal of Power Electronics*, vol. 17, no. 5, pp. 1223-1230, 2017.
[**DOI:**10.6113/JPE.2017.17.5.1223]

[27] S. Mu, J. Kang, Z. Zhong, Z. Ma, “Improved detecting method for multiple rotating reference frames based harmonic control of PMSMs”, *Chinese Automation Congress (CAC)*, pp. 5458-5463, pp. 2020.
[**DOI:** 10.1109/CAC51589.2020.9327812]

[28] J. Taylor, D.F. Valencia Garcia, W. Taha, M. Mohamadian, “Dynamic Modelling of Multiphase Machines Based on the VSD Transformation,” *SAE Technical Paper 2021-01-0774*, doi:10.4271/2021-01-0774, 2021.
[**DOI:**10.4271/2021-01-0774]

[29] A. Halvaei Niasar, M. Ahmadi, S.H. Edjtahed, “Sensorless Control of Non-Sinusoidal Permanent Magnet Brushless Motor Using Selective Torque Harmonic Elimination Control Method Based on Full-Order Sliding Mode Observer”, *Advances in Power Electronics Journal*, vol. 2016, no. 9358604, pp. 1-13, 2016.
[**DOI**:10.1155/2016/9358604]

[30] D.G. Luenberger, Y. Ye, “Linear and Nonlinear Programming,” *Springer*, 2008.
[**DOI:** 10.2307/1240727]

[31] 24H. Ghanayem, M. Alathamneh, R.M. Nelms, “A Comparative Study of PMSM Torque Control using Proportional-Integral and Proportional-Resonant Controllers”, *IEEE SoutheastCon*, pp. 453-458, 2022.
[**DOI:** 10.1109/SoutheastCon48659.2022.9764111]

[32] 25H. Park, T. Kim, Y. Suh, “Fault-Tolerant Control Methods for Reduced Torque Ripple of Multiphase BLDC Motor Drive System Under Open-Circuit Faults”, *IEEE Trans. on Industry Applications*, vol. 58, no. 6, pp. 7275-7285, Nov./Dec. 2022.
[**DOI:** 10.1109/TIA.2022.3191633]

Davood Maleki, was born in 1980 in Malayer, Iran. He received a Bachelor's degree in Electronics and a Master's degree in Electrical Machines from Malek Ashtar Industrial University in Shahin Shahr, Isfahan. His Bachelor's thesis was on the design of a buck-boost regulator for a 400 to 24 converter, and His Master's thesis focused on the construction of an LSPMSM drive. He is currently a PhD student at University of Kashan. His interests are control and implementation of multi-phase PMSM drives.

Abolfazl Halvaei Niasar, (S’04–M’06–SM’14) was born in Kashan, Iran in 1974. He received his B.Sc., M.Sc., and Ph.D. in 1996, 1999, and 2008 from Isfahan University of Technology (IUT), University of Tehran (UT) and Iran University of Science and Technology (IUST) respectively, all in electrical engineering. He has joined the Department of Electrical and Computer Engineering at University of Kashan, Kashan, Iran since 2008 as assistant professor. He has authored more than 150 technical papers published in journals and conference proceedings. He is the holder of two Iranian patents and has directed some industrial research projects in field of electrical drives. His current major research interests include PM and brushless DC motor (BLDC) drives, sensorless drives, design, analysis and control of electrical machines. Dr. Halvaei is senior member of the Institute of Electrical and Electronics Engineers, IEEE.